Herschel: the first science highlights

Astronomy & Astrophysics

Special feature

Letter to the Editor

Dust, Ice, and Gas In Time (DIGIT) *Herschel*[*] program first results

A full PACS-SED scan of the gas line emission in protostar DK Chamaeleontis

T. A. van Kempen[1], J. D. Green[2], N. J. Evans II[2], E. F. van Dishoeck[3,4], L. E. Kristensen[3], G. J. Herczeg[4], B. Merín[5], J.-E. Lee[6], J. K. Jørgensen[7], J. Bouwman[8], B. Acke[9,24], M. Adamkovics[10], J. C. Augereau[11], E. Bergin[12], G. A. Blake[13], J. M. Brown[4], J. S. Carr[14], J.-H. Chen[2], L. Cieza[15], C. Dominik[16,17], C. P. Dullemond[8,18], M. M. Dunham[2], A. Glassgold[10], M. Güdel[19], P. M. Harvey[2], Th. Henning[8], M. R. Hogerheijde[3], D. Jaffe[2], H. J. Kim[2], C. Knez[20], J. H. Lacy[2], S. Maret[11], G. Meeus[21], R. Meijerink[3], G. D. Mulders[16,22], L. Mundy[20], J. Najita[23], J. Olofsson[8], K. M. Pontoppidan[13], C. Salyk[2], B. Sturm[8], R. Visser[3], L. B. F. M. Waters[9,16], C. Waelkens[9], and U. A. Yıldız[3]

(Affiliations are available in the online edition)

ABSTRACT

Aims. We aim to study the composition and energetics of the circumstellar material of DK Cha, an intermediate-mass star in transition from an embedded configuration to a star plus disk stage, during this pivotal stage of its evolution.
Methods. Using the range scan mode of PACS on the *Herschel* Space Observatory, we obtained a spectrum of DK Cha from 55 to 210 μm as part of the DIGIT key program.
Results. Almost 50 molecular and atomic lines were detected, many more than the 7 lines detected in ISO-LWS. Nearly the entire ladder of CO from $J = 14$–13 to 38–37 ($E_u/k = 4080$ K), water from levels as excited as $J_{K_{-1}K_{+1}} = 7_{07}$ ($E_u/k = 843$ K), and OH lines up to $E_u/k = 290$ K were detected.
Conclusions. The continuum emission in our PACS SED scan matches the flux expected by a model consisting of a star, a surrounding disk of 0.03 $M_\odot$, and an envelope of a similar mass, supporting the suggestion that the object is emerging from its main accretion stage. Molecular, atomic, and ionic emission lines in the far-infrared reveal the outflow's influence on the envelope. The inferred hot gas may be photon-heated, but some emission may be caused by C-shocks in the walls of the outflow cavity.

Key words. astrochemistry – circumstellar matter – stars: formation – stars: protostars – infrared: ISM – submillimeter: ISM

1. Introduction

One of the pivotal points in the formation of a star occurs when the star and disk system emerges from the collapsing envelope, signaling the end of the main accretion of stellar mass. The transition from a stage I protostar, embedded in a substantial envelope, to a stage II configuration, with only a star and disk[1], is poorly understood.

At a distance of 178 ± 18 pc IRAS 12496-7650 is the brightest infrared (IR) and submillimeter (submm) source in the Chamaeleon II star-forming region, (Whittet et al. 1997). Follow-up studies to the discovery of IRAS 12496-7650 by Hughes et al. (1989, 1991), along with subsequent observations (e.g., Whittet et al. 1997; Young et al. 2005; Porras et al. 2007; Spezzi et al. 2008), identified the variable Herbig Ae star DK Cha as the optical counterpart. The central star mass is estimated to be 2–3 $M_\odot$ (Spezzi et al. 2008) with a bolometric luminosity between 24 (Spezzi et al. 2008) and 35 $L_\odot$ (van Kempen et al. 2009a). The star is surrounded by a molecular outflow and

protostellar envelope (van Kempen et al. 2006; van Kempen et al. 2009a). The spectral energy distribution (SED) is roughly flat with wavelength from the near-infrared to mid-infrared (Hughes et al. 1989). Using the T_{bol} definition and including longer wavelength data (e.g., Henning et al. 1993; van Kempen et al. 2009a), DK Cha has $T_{bol} = 580$ K, making it a class I source, but near the class II boundary at 650 K. Owing to an approximately face-on viewing angle down the outflow cone (van Kempen et al. 2009a), one can observe the protostellar disk directly, unobstructed by the surrounding envelope. This viewing angle also allows the optical emission to escape. The observational SED classes are often assumed to correspond to the physical stages, but this is by no means obvious when aspherical models are examined (e.g., Robitaille et al. 2007; Crapsi et al. 2008; Dunham et al. 2010) or tracers of dense gas are considered (van Kempen et al. 2009b). The same physical object can have different SED classifications depending on the viewing angle. Thus, it is interesting to study an object that is near an SED classification boundary and that also appears to be transitional in physical stage.

Strong far-IR continuum and line emission have been detected (Giannini et al. 1999; van Kempen et al. 2006). As discussed by van Dishoeck (2004); Nisini et al. (2005), and

---

[1] See, e.g., Robitaille et al. (2007) for a definition of the stages.

van Kempen et al. ([2010](#)) for the similar source HH46, far-IR atomic, ionic, and molecular lines can constrain the properties of the disk, envelope, and outflow. The CO emission lines between $J = 14$–13 and $J = 19$–18, as well as [O I] and [C II], were observed from DK Cha with ISO-LWS, but other possible molecular species, such as OH and H_2O, were undetected ([Lorenzetti et al. 1999](#); [Giannini et al. 1999](#)).

The large beam of ISO-LWS (90″) and its low spectral resolving power ($\lambda/\Delta\lambda = 200$) were insufficient to determine the origin (e.g., envelope versus outflow) of the CO emission. The preferred picture was of a small, quiescent hot core of ~300 AU around the protostar ([Giannini et al. 1999](#)), but observations of CO 4–3 and 7–6 indicate that this warm CO emission either originates outside the inner few thousand AU or cannot be heated simply by radiation from the central star (passive heating) ([van Kempen et al. 2006](#)); the far-IR and submm lines have different energies and critical densities, so they may originate in different regions.

The *Herschel* key programme Dust, Ice, and Gas In Time (DIGIT) aims to study the evolution of these three constituents through the star formation process by observing objects at different stages. This paper, along with a companion paper on HD100546, a stage II object ([Sturm et al. 2010](#)), present the first results from the DIGIT science demonstration observations.

2. Observations

The launch of the *Herschel* Space Observatory ([Pilbratt 2010](#)) with the Photodetector Array Camera and Spectrometer (PACS) instrument ([Poglitsch 2010](#)) oboard, enables the acquisition of far-IR spectra with high spectral resolving power and good spatial ($\sim9''$) resolution. The range scan/SED mode provides a full spectrum (55–$210\,\mu$m).

DK Cha was observed for a total of ~4 h on 10 December 2009 by the PACS spectrometer on the *Herschel* Space Observatory in pointed range-scan spectroscopy mode (obsid 1342188039 and 1342188040). An image slicer rearranges the light within a 5×5 array, with each spatial pixel (spaxel) covering $9''.4 \times 9''.4$. A grating disperses the light onto two 16×25 pixel Ge:Ga detectors. Observations were taken using nodding, in which two off-positions separated by ±6 arcmin in elevation were taken as "blank" sky, from which the signal is subtracted. Consequently, spatially diffuse lines (e.g., [C II]) are subtracted out.

The effective spectral resolving power was about $1000+/-500$, lower than expected, because of the pointing error, which is perpendicular to the slit, and the effects of fringing on the continuum. The point-spread function of PACS increases towards longer wavelengths and is larger than a single spaxel, but is corrected in post-processing using the PACS spectrum of the point-like HD100546 ([Sturm et al. 2010](#)) to calculate the extraction efficiencies.

The data were reduced using the *Herschel* interactive processing environment (HIPE v. 2.4). The observation was slightly mispointed (~5–$6''$) making it difficult to assess whether the emission is extended and causes wavelength shifts in some spectral ranges. Because of the mispointing, uncertainty in the spectral response function, light leakage problems, and uncertainties in the wavelength dependence of the PSF, the spectrum was trimmed shortward of 56 μm, longward of 190 μm, and in the range 95–101 μm. Two spectra were used to identify lines: One from the central spaxel alone and a second spectrum, which was used for most lines, craeted by summing the fluxes from all spatial pixels to correct for the PSF and mispointing. We focus on gas lines in this Letter.

Table 1. Detected gas lines within the PACS spectrum of DK Cha.

Species	Transition	λ^a μm	E_u K	FWHM μm	Flux[b] W m^{-2}
[O I]	$^3P_1$-$^3P_2$	63.18	227.72	0.08	3657.7
OH 3/2-3/2	9/2- – 7/2+	65.13	512.1	0.05	56.0[2]
OH 3/2-3/2	9/2+ – 7/2-	65.28	510.9	0.07	52.3[2]
CO	38-37	69.07	4079.98	0.06	42.1[2]
CO	37-36	70.91	3871.88	0.09	59.6[2]
o-H$_2$O[3]	7_{07}-6_{16}	71.95	843.5	0.06	37.1[2]
CO	36–35	72.84	3668.96	0.06	40.1[2]
CO	35–34	74.89	3471.44	0.1	57.0[2]
o-H$_2$O	4_{23}-3_{12}	78.74	432.2	0.04	19.8[2]
OH 1/2-3/2	1/2- – 3/2+	79.12	181.7	0.06	28[2]
CO	33–32	79.36	3092.45	0.03	17.5[2]
CO	32-31	81.81	2911.15	0.05	126.2
o-H$_2$O	6_{16}-5_{05}	82.09	643.5	0.03	96.2
CO	31–30	84.41	2735.28	0.09	336.0
OH 3/2-3/2	7/2+ – 5/2-	84.42[1]	291.2	–	–
OH 3/2-3/2	7/2- – 5/2+	84.60	290.5	0.09	301.4
CO	30–29	87.19	2564.94	0.09	317.5
CO	29–28	90.16	2399.93	0.14	545.8
CO	28–27	93.35	2240.30	0.07	261.4
CO	27–26	96.77	2086.22	0.10	330.1
CO	25–24	104.44	1794.23	0.2	314.5
o-H$_2$O	2_{21}-1_{10}	108.08	194.1	0.15	126.9
CO	24–23	108.76	1656.55	0.15	260.0
CO	23–22	113.46	1524.19	0.2	477.4
o-H$_2$O	4_{14}-3_{03}	113.54[1]	323.5	–	–
CO	22–21	118.58	1397.43	0.17	285.2
OH 3/2-3/2	5/2- – 3/2+	119.23	120.7	0.18	<40
OH 3/2-3/2	5/2+ – 3/2-	119.44	120.5	0.17	<72.3
[N II]	$^3P_2$-$^3P_1$	121.90	188.20	0.12	45.7
CO	21–20	124.19	1276.10	0.17	357.1
p-H$_2$O	4_{04}-3_{13}	125.35	319.5	0.12	42.8
CO	20–19	130.37	1160.24	0.16	319.0
CO	19–18	137.20	1049.89	0.18	338.7
p-H$_2$O	3_{13}-2_{02}	138.53	204.7	0.17	103.0
CO	18–17	144.78	945.01	0.15	350.4
[O I]	$^3P_0$-$^3P_2$	145.53	326.58	0.16	146.7
CO	17–16	153.27	845.63	0.15	386.0
CO	16–15	162.81	751.76	0.18	466.5
OH 1/2-1/2	3/2+ – 1/2-	163.12	270.2	0.24	91.0
OH 1/2-1/2	3/2+ – 1/2-	163.40	269.8	0.19	90.0
CO	15–14	173.63	663.37	0.16	413.0
o-H$_2$O	3_{03}-2_{12}	174.63	196.8	0.19	208.0
o-H$_2$O	2_{12}-1_{01}	179.53	114.4	0.11	31.0
o-H$_2$O	2_{21}-2_{12}	180.49	194.1	0.12	34.9
CO	14–13	186.00	580.51	0.20	437.2

Notes. [a] Laboratory wavelength; [b] flux summed over all pixels in 10^{-18} W m^{-2}. Typical line flux uncertainties are dominated by calibration uncertainties (~30–50%) and fringing (0.1 Jy at the longest wavelengths to 0.6 Jy at the shortest); [1] lines blended with above line; [2] Line detected only in central spaxel and should not be compared to the fluxes of the summed spaxels; [3] doublet unresolved.

3. Results

3.1. Continuum

The total SED in Fig. [1](#) includes photometry from the literature ([Alcalá et al. 2008](#); [Spezzi et al. 2008](#); [Evans et al. 2009](#), Nefs et al., in prep), combined with *Spitzer*-IRS spectroscopy and the PACS results. The photometric points were fitted by the SED fitter routine from [Robitaille et al. (2007)](#), the resultin parameters being shown in Table [2](#). Because of the the extinction and variability at short wavelengths, only points longwards of 3 μm were considered as input to the fit. The best-fit model is overplotted and divided into the contributions from the star, disk, and envelope. The short-wavelength IRS continuum is dominated by the flux from the disk, the longer wavelength IRS continuum covers
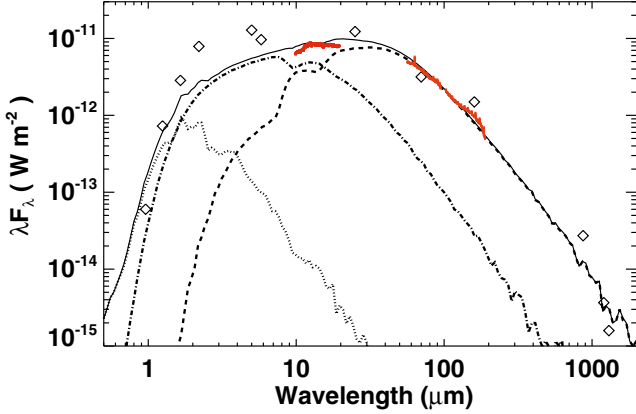
Fig. 1. SED of DK Cha using WFI *I*-band data, 2MASS (*J, H, K*) and *Spitzer*-IRAC (3.6 and 4.5 μm. The other bands, 5.8 and 8.0 μm not being shown due to saturation), *Spitzer*-MIPS (24, 70 and 160 μm), APEX-Laboca (870 μm) and SEST (1.2 and 1.3 mm). Overplotted are the best-fit model from the Robitaille et al. (2007) grid and the PACS and *Spitzer*-IRS spectra. The MIPS 70 μm is corrected for saturation; the 160 μm for large-scale emission. The solid line is the full model, while the dashed line shows the envelope contribution, the dot-dashed the disk contribution, and the dotted that of the star. Photometric points are shown as diamonds. The short-wavelength points are not well matched. Fluxes at short wavelength (<3 μm) are variable.

Table 2. Best-fit from Robitaille models.

DK Cha characteristics			
Envelope mass	0.03 $M_\odot$	A_V[1]	7.9
Disk mass	0.03 $M_\odot$	Inclination	<18°
Luminosity	29.4 $L_\odot$	Disk Inner Radius	0.3 AU

Notes. [1] Total A_v of which A_v = 5.2 mag. is attributed to the envelope at an inclination of 18° and 2.7 mag. to more extended cloud.

the transition from disk to envelope, and the PACS continuum arises in the envelope. The model underestimates the observations in the near-IR and mid-IR, indicating that the disk emission is underestimated in the model.

The best-fit models of the SED grid indeed confirm the assumption of a nearly face-on configuration <18° with relatively low and equal envelope and disk masses of 0.03 $M_\odot$, indicative of a source in transition from stage I to stage II (Robitaille et al. 2007). The PACS continuum was not used to constrain the fit, the consistency with the predicted model (differences of <10%) thus being encouraging, especially considering the calibration uncertainty of 30–50%.

3.2. Line inventory

Table 1 lists all gas lines that have been identified. Figure 2 shows the spectrum after subtraction of a polynomial fit to the continuum. We used a combination of the ISO line list[2] and the list published in Lerate et al. (2006) for the Orion bar. More lines may be detectable in this spectrum after PSF deconvolution. Some lines in Table 1 are only detected in the central spaxel. Owing to the fringing in other spaxels at short wavelengths and the PSF problems discussed above, these lines cannot be seen in the summed result of Fig. 2. Using spectra from both the summation of all 25 spaxels and from only the central spaxel, a large range of CO, H_2O, and OH lines were detected, ranging in

---

[2] http://www.mpe-garching.mpg.de/iso/linelists/Molecular.html

---

excitation energies from a few hundred kelvin to over 3000 K. In addition, [O I] and [N II] were identified. Emission from [C II] at 157.7 μm is not seen. That line was detected by Lorenzetti et al. (1999), but was interpreted to be extended emission, associated with the galactic ISM. This component is subtracted out in our observations due to the nodding, which was not used in ISO-LWS.

3.3. Gas analysis

infrared CO lines were previously detected by Giannini et al. (1999), but only up to CO J = 19–18. Assuming the lines to be optically thin, those could be fitted with temperatures ranging from T = 200 K to T = 750 K and densities from $n = 4 \times 10^6$ cm^{-3} to $n = 5 \times 10^5$ cm^{-3}. The high T, low n model, which produces the most emission in the high-J lines, is overplotted in Fig. 3. As can be seen, this model severely underpredicts the intensity of the CO lines from higher transitions seen by *Herschel*. The other proposed models predict even less high-J emission.

The CO level populations up to J = 31 (Fig. 3), can be fitted with two distinct rotational temperatures (T_{Rot}), a break occurring at about E_{up} = 1500 K. Most of the mid-J CO lines can be fitted by $T_{Rot} \sim 380$ K, while higher excitation lines are best fitted with $T_{Rot} \sim 1365$ K. In HH46 (van Kempen et al. 2010), UV photon heating (Spaans et al. 1995) predominates for lines with energies below 1700 K, while a non-dissociative C-shock has a more important effect than the emission from higher excitation lines. A similar model is plausible for DK Cha, but this issue will be explored in a forthcoming paper (Green et al. in prep).

Water was detected in a wide variety of transitions, up to 7_{07}–6_{16} at 71.93 μm with (E/k = 843 K). Water was not detected in ISO-LWS (Giannini et al. 1999) because the lines are 5 times weaker than the CO lines. The discovery of the 7_{07}–6_{16} line is indicative of high temperature, as confirmed by the high-J CO lines. Given the possible identification of shocked CO and the geometry of DK Cha, it is likely that the water emission arises at least in part from either a non-dissociative C-shock or UV-heating of the quiescent material along the outflow cavity walls.

In addition, at least 9 lines of OH are detected. Since oxygen is rapidly transformed into H_2O at temperatures higher than 100 K and frozen out below that, either a very strong UV field or a dissociative shock is needed. OH is a major coolant for dissociative shocks (Neufeld & Dalgarno 1989). This dissociative shock is accompanied by a C-shock, which may explain the CO and H_2O analysis. Models from Wampfler et al. (in prep) also suggest that C-shock densities are often too low to account for both these high excitation lines and at the same time not overproduce the 119 and 163 μm OH lines.

HD 100546 (Sturm et al. 2010), a Herbig Be star without an envelope, was chosen for early observations to be a source analogous to DK Cha, but more evolved. A comparison is useful because similar species are seen in its spectrum. Emission of H_2O and OH from the upper layers of a flared, but quiescent disk, similar to that around HD 100546 (Sturm et al. 2010), may account for some of the lines from DK Cha. However, accounting for the difference in distance, the CO lines from DK Cha are more than 10 times stronger, and higher excitation lines from H_2O are seen toward DK Cha.

A possible explanation of the stronger emission of DK Cha is an accretion shock onto the disk, where high densities and temperatures are present. Another possibility is a shock in the walls of the outflow, which will also be examined further in Green et al. (in prep.).

Fig. 2. The spectrum from 55–190 μm of all spaxels added together, after removal of the continuum and rebinning to 0.5 μm resolution. Several dips or bumps (e.g., around 75 μm) are instrument artifacts. Inserts show expanded views of parts of the spectrum, with line identifications.

Fig. 3. *Upper*: CO line fluxes plotted versus J_{up}. The ISO line fluxes are shown with triangles. A clear excess can be seen in the CO line fluxes from $J_{up} = 20$ onwards compared to the warmest model of 750 K proposed by Giannini et al. (1999) (dashed line). *Lower*: CO Rotational diagram, showing two distinct populations with a break around 1500 K in energy. The blended lines are excluded from the fit and the plot. CO lines with J_{up} larger than 31 are excluded from both plots, as these lines are detected only in the central spaxel.

4. Conclusions

We have found that the continuum models that fit the data of DK Cha are consistent with the interpretation that it is a transitional objsect between a stage I and stage II, with nearly equal masses in the envelope and disk and a nearly face-on geometry. The full PACS SED mode observations reveal an extremely rich spectrum of over 50 ionic, atomic, and molecular lines. With additional improvements to the spectral response function, we will be able to identify additional gas, ice, and dust features in the spectrum. The full range scan/SED mode will be able to probe many aspects of a protostellar object, from the ambient envelope to gas excited by ultraviolet radiation and by shocks.

References

Alcalá, J. M., Spezzi, L., Chapman, N., et al. 2008, ApJ, 676, 427
Crapsi, A., van Dishoeck, E. F., Hogerheijde, M. R., Pontoppidan, K. M., & Dullemond, C. P. 2008, A&A, 486, 245
Dunham, M. M., Evans, N. J., Terebey, S., Dullemond, C. P., & Young, C. H. 2010, ApJ, 710, 470
Evans, N. J., Dunham, M. M., Jørgensen, J. K., et al. 2009, ApJS, 181, 321
Giannini, T., Lorenzetti, D., Tommasi, E., et al. 1999, A&A, 346, 617
Henning, T., Pfau, W., Zinnecker, H., & Prusti, T. 1993, A&A, 276, 129
Hughes, J. D., Emerson, J. P., Zinnecker, H., & Whitelock, P. A. 1989, MNRAS, 236, 117
Hughes, J. D., Hartigan, P., Graham, J. A., Emerson, J. P., & Marang, F. 1991, AJ, 101, 1013
Lerate, M. R., Barlow, M. J., Swinyard, B. M., et al. 2006, MNRAS, 370, 597
Lorenzetti, D., Tommasi, E., Giannini, T., et al. 1999, A&A, 346, 604
Neufeld, D. A., & Dalgarno, A. 1989, ApJ, 340, 869
Nisini, B., Antoniucci, S., Giannini, T., & Lorenzetti, D. 2005, A&A, 429, 543
Pilbratt, G. L., Riedinger, J. L., Passvogel, T., et al. 2010, A&A, 518, L1
Poglitsch, A., Waelkens, C., Geis, N., et al. 2010, A&A, 518, L2
Porras, A., Jørgensen, J. K., Allen, L. E., et al. 2007, ApJ, 656, 493
Robitaille, T. P., Whitney, B. A., Indebetouw, R., & Wood, K. 2007, ApJS, 169, 328
Spaans, M., Hogerheijde, M. R., Mundy, L. G., & van Dishoeck, E. F. 1995, ApJ, 455, L167
Spezzi, L., Alcalá, J. M., Covino, E., et al. 2008, ApJ, 680, 1295
Sturm, B., Bouwman, J., Henning, Th. et al. 2010, A&A, 518, L129
van Dishoeck, E. F. 2004, ARA&A, 42, 119
van Kempen, T. A., Hogerheijde, M. R., van Dishoeck, E. F., et al. 2006, A&A, 454, L75
van Kempen, T. A., van Dishoeck, E. F., Hogerheijde, M. R., & Güsten, R. 2009a, A&A, 508, 259
van Kempen, T. A., van Dishoeck, E. F., Salter, D. M., et al. 2009b, A&A, 498, 167
van Kempen, T. A., Kristensen, L. E, Herzceg, G. J, et al. 2010, A&A, 518, L121
Whittet, D. C. B., Prusti, T., Franco, G. A. P., et al. 1997, A&A, 327, 1194
Young, K. E., Harvey, P. M., Brooke, T. Y., et al. 2005, ApJ, 628, 283

Page 5 is available in the electronic edition of the journal at http://www.aanda.org

[1] Harvard-Smithsonian Center for Astrophysics, 60 Garden Street, MS 78, Cambridge, MA 02138, USA
e-mail: tvankempen@cfa.harvard.edu

[2] The University of Texas at Austin, Department of Astronomy, 1 University Station C1400, Austin, Texas 78712-0259, USA

[3] Leiden Observatory, Leiden University, PO Box 9513, 2300 RA Leiden, The Netherlands

[4] Max-Planck-Institut für extraterrestriche Physik. Garching, Germany

[5] *Herschel* Science Centre, European Space Astronomy Centre (ESA), PO Box 78, 28691 Villanueva de la Cañada (Madrid), Spain

[6] Department of Astronomy and Space Science, Astrophysical Research Center for the Structure and Evolution of the Cosmos, Sejong University, Seoul 143-747, Republic of Korea

[7] Centre for Star and Planet Formation, Natural History Museum of Denmark, University of Copenhagen, Øster Voldgade 5-7, 1350 Copenhagen K., Denmark

[8] Max Planck Institute for Astronomy, Königstuhl 17, 69117 Heidelberg, Germany

[9] Instituut voor Sterrenkunde, K.U. Leuven, Celestijnenlaan 200D, 3001 Leuven, Belgium

[10] Astronomy Department, University of California, Berkeley, CA 94720, USA

[11] Laboratoire d'Astrophysique de Grenoble, CNRS/Université Joseph Fourier (UMR5571) BP 53, 38041 Grenoble Cedex 9, France

[12] Department of Astronomy, The University of Michigan, 500 Church Street, Ann Arbor, MI 48109-1042, USA

[13] Caltech, Division of Geological & Planetary Sciences, Mail Code 150-21, Pasadena, CA 91125

[14] Naval Research Laboratory, Code 7211, Washington, DC 20375, USA

[15] Institute for Astronomy, University of Hawaii at Manoa, Honolulu, HI 96822, USA ; *Spitzer* Fellow

[16] Astronomical Institute "Anton Pannekoek", University of Amsterdam, PO Box 94249, 1090 GE Amsterdam, The Netherlands

[17] Department of Astrophysics/IMAPP, Radboud University Nijmegen, PO Box 9010 6500 GL Nijmegen, The Netherlands

[18] Institut für Theoretische Astrophysik, Universitt Heidelberg, Albert-Ueberle-Strasse 2, 69120 Heidelberg, Germany

[19] University of Vienna, Department of Astronomy, Türkenschanzstr. 17, 1180 Vienna, Austria

[20] Department of Astronomy, University of Maryland, College Park, MD 20742, USA

[21] Dpt. de Física Teórica, Fac. de Ciencias, Universidad Autónoma de Madrid, Cantoblanco, 28049 Madrid, Spain

[22] SRON Netherlands Institute for Space Research, PO Box 800, 9700 AV, Groningen, The Netherlands

[23] National Optical Astronomy Observatory, 950 N. Cherry Ave., Tucson, AZ 85719, USA

[24] Postdoctoral Fellow of the Fund for Scientific Research, Flanders, Belgium